AIAA 80-0190R

Navier-Stokes Solution of a Slender Body of Revolution at Incidence

W. L. Hankey,* J. E. Graham,† and J. S. Shang‡
Air Force Wright Aeronautical Laboratories, Wright-Patterson Air Force Base, Ohio

The three-dimensional flowfield surrounding an ogive cylinder at angle of attack is solved through integration of the complete Navier-Stokes equations. The leeside vortex pattern is computed for a three caliber ogive cylinder at Mach number 1.98. Laterally-symmetric three-dimensional flowfields are obtained on a CRAY-1 computer in 40 min utilizing MacCormack's algorithm as vectorized by Shang. The computed results compare favorably with the experimental data in that all primary features are captured.

Nomenclature

d = diameter of ogive
e = specific internal energy, $C_v T + (u^2 + v^2 + w^2)/2$
E,F,G = vector fluxes
k = exponential stretching factor (radial direction)
L = length of ogive (in the x direction)
n = outward normal from ogive body
p = static pressure
$\dot{q}$ = rate of heat transfer
r = spherical radius (distance from apex of ogive body)
R = radius of the ogive body
R_B = outer boundary radius (distance from x axis to outer radial boundary)
R_f = field point radius (distance from x axis to a given field point)
Re = Reynolds number based on running length, $\rho_\infty u_\infty x/\mu_\infty$
t = time
T = static temperature
u,v,w = velocity components in the Cartesian frame
U = dependent variables in vector form (ρ, ρu, ρv, ρw, ρe)
V = velocity vector ($u\hat{i} + v\hat{j} + w\hat{k}$)
x,y,z = coordinate in the Cartesian frame
α = angle of attack
ϵ = downwash angle [angle between freestream velocity vector and a given field velocity vector, i.e., $\epsilon = \alpha - \tan^{-1}(v/u)$]
ξ,η,ζ = transformed coordinate system
ρ = density
θ = radial angle around ogive
$\underline{\underline{\tau}}$ = stress tensor

Subscripts

$\underline{\underline{(\ )}}$ = tensor
tr = transition

Introduction

EXPERIMENTAL studies[1-6] on slender bodies at high angle of attack have identified the existence of unusual flowfield phenomena. At small angles of attack (<25 deg) and for small cross flow Mach numbers,[7] a pair of stationary symmetric vortices appear on the leeward side (Fig. 1). For higher angles of attack ($30 < \alpha < 60$ deg), several pairs of asymmetrical vortices exist on high fineness ratio bodies. Generally these vortices are also stationary, although intermittent regions of unsteadiness have been observed. At even higher angles of attack the shedding vortices become completely unsteady. The steady asymmetric case is of considerable interest to the aircraft industry since large side forces (experienced at zero yaw angles) are capable of producing aircraft departure into a spin situation. Although this phenomenon has been known for several decades, no reliable analytical prediction method exists. Recently, however, advances have occurred in the numerical solution of the Navier-Stokes equations for solving complex viscous flows. These solutions generally have been for two-dimensional flows, while the computation of the vortex fields generated by slender bodies at angle of attack requires the use of the three-dimensional Navier-Stokes equations, although attempts at using the parabolized Navier-Stokes equations have shown some success.[8] The practicality of three-dimensional calculations can be achieved through the use of vector processor computers (CRAY, STAR, Illiac) developed only recently. This practicality can be demonstrated by considering a typical three-dimensional problem with a grid of $15 \times 30 \times 30$ points for which 4000 time steps are required to obtain convergence, which were the figures obtained for the current problem. Convergence criteria for the current problem initially consisted of graphical comparisons that were verified numerically by a lack of change in the dependent variables (i.e., less than 2% change in pressure over one characteristic time). Based upon the timing results of the benchmark computations of Ref. 9 (for three-dimensional Navier-Stokes solutions using MacCormack's[10] method), estimates of the computational time for this typical three-dimensional problem on three different class computers can be obtained.

Table 1 dramatically shows the recent improvement in computer efficiency thereby making three-dimensional Navier-Stokes calculations feasible. Because of the availability of the CRAY-1 computer through remote access, a numerical investigation of slender body flowfields was initiated based on the importance of unpredictable yawing moments on aircraft and missiles. Using a previously

Table 1 Benchmark computations[7]

Computer version	Computer time
CDC 6600	36 h
CDC 7600	7 h
CRAY-1	46 min

Presented as Paper 80-0190 at the 19th Aerospace Sciences Meeting, St. Louis, Mo., Jan. 12-15, 1981; submitted Feb. 20, 1981; revision received June 29, 1981. This paper is declared a work of the U. S. Government and therefore is in the public domain.

*Senior Scientist. Associate Fellow AIAA.
†Mathematician.
‡Aerospace Engineer. Associate Fellow AIAA.

developed vectorized Navier-Stokes code,[11] a program was initiated to compute the entire flowfield over slender bodies at angle of attack. Two phases are contemplated. First, symmetric vortices are to be investigated, both laminar and turbulent. Second, larger angles of attack will be examined in which the asymmetric situation develops. This paper addresses only the laminar calculations of the first phase.

Method of Solution

A body-oriented coordinate transformation is utilized to map the x,y,z physical space (Fig. 2) into a unit cube in the ξ,η,ζ transformed space (Fig. 3). A uniform set of grid points in the transformed space permits the implementation of simple finite-difference relationships whose image in the physical space is a highly nonuniform grid capable of resolving significant flowfield features.

The transformation relationship used for the ogive cylinder was defined first for the cylindrical portion of the body as follows.

$$\xi=\xi(x)$$

$$\eta=\frac{1}{k}\ell n\left[\frac{R_f(e^k-1)+R_B-Re^k}{R_B-R}\right]$$

$$\zeta=\theta/\pi$$

where $\xi(x)$ spaced the cross flow stations geometrically to include the location of the experimentally measured data planes in the computation. The ogive nose portion was described by a family of ogive curves of common origin with increasing radius (see Fig. 2).

The three-dimensional, compressible Navier-Stokes equations are given as[9]

$$\frac{\partial U}{\partial t}+\frac{\partial E}{\partial x}+\frac{\partial F}{\partial y}+\frac{\partial G}{\partial z}=0$$

where the flux vectors are the following:

$$U=\begin{vmatrix}\rho\\ \rho u\\ \rho v\\ \rho w\\ \rho e\end{vmatrix}\qquad E=\begin{vmatrix}\rho u\\ \rho u^2-\sigma_{xx}\\ \rho uv-\tau_{xy}\\ \rho uw-\tau_{xz}\\ \rho ue-(\dot{V}\cdot\underline{\tau})_x-\dot{q}_x\end{vmatrix}$$

$$F=\begin{vmatrix}\rho v\\ \rho uv-\tau_{xy}\\ \rho v^2-\sigma_{yy}\\ \rho vw-\tau_{yz}\\ \rho ve-(\dot{V}\cdot\underline{\tau})_y-\dot{q}_y\end{vmatrix}$$

$$G=\begin{vmatrix}\rho w\\ \rho uw-\tau_{xz}\\ \rho vw-\tau_{yz}\\ \rho w^2-\sigma_{zz}\\ \rho we-(\dot{V}\cdot\underline{\tau})_z-\dot{q}_z\end{vmatrix}$$

The transformed equations for the ogive-cylinder become

$$\frac{\partial U}{\partial t}+\xi_x\frac{\partial E}{\partial\xi}+\left(\eta_x\frac{\partial E}{\partial\eta}+\eta_y\frac{\partial F}{\partial\eta}+\eta_z\frac{\partial G}{\partial\eta}\right)+\left(\zeta_y\frac{\partial F}{\partial\zeta}+\zeta_z\frac{\partial G}{\partial\zeta}\right)=0$$

The explicit finite-difference method of MacCormack[10] (unsplit version), as vectorized for the CRAY computer by Shang[11] is employed to obtain a steady-state solution through integration in time from some initial guess. The method is second-order accurate throughout but is conditionally stable subject to CFL (Courant-Friedrichs-Lewy) time step restriction.

Boundary Conditions

Boundary conditions must be prescribed on the six faces of the cube in the transformed space (see Fig. 3). These faces are the 1) upstream and 2) downstream planes, 3) wall surface, 4) far field boundary, and 5) and 6) two faces on the plane of symmetry.

The following boundary conditions are applied after each iteration, which consists of sweeps in all three directions.

1) Upstream Face: In the interest of computational economy a "locally-conical" viscous solution (as originated by McRae[12]) was calculated for a short cone ($L<d$) through the implementation of a Neumann condition on the upstream face of the ogive-cylinder body

$$\frac{\partial U}{\partial r}(t,\xi_0,\eta,\zeta)=0$$

where r is the spherical radius emanating from the apex of the ogive. By choosing a grid that is conically symmetric at the

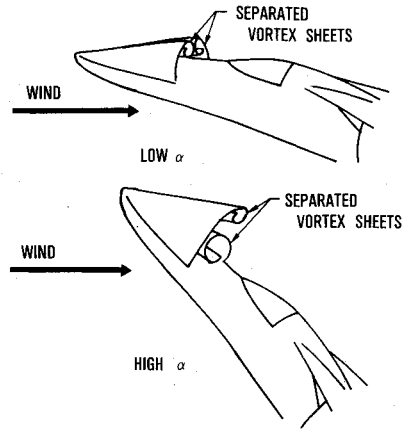

Fig. 1 Sketch of flow phenomena.[1]

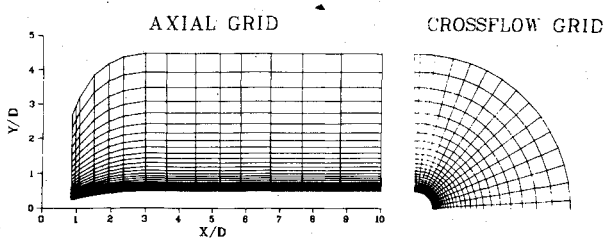

Fig. 2 Computational grid (physical space).

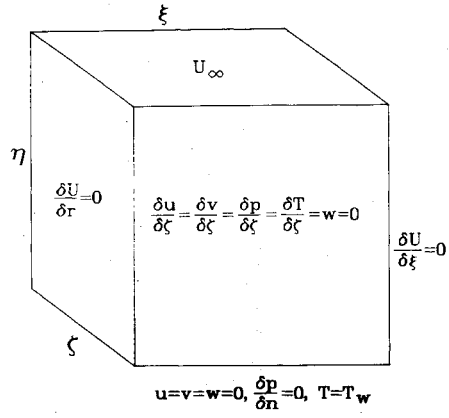

Fig. 3 Boundary conditions (transformed space).

origin

$$\left(\frac{\partial}{\partial \xi}\right)_0 = \left(\frac{\partial}{\partial r}\right)_0$$

2) Downstream Face: For supersonic flow approaching an asymptotic state, experience indicates that a simple vanishing gradient condition on a downstream boundary is generally satisfactory.

$$\frac{\partial U}{\partial \xi}(t, \xi_L, \eta, \zeta) = 0$$

3) Wall: On the surface a no-slip condition was used for the velocity components along with a prescribed wall temperature. The pressure (which cannot be determined through a boundary condition) is computed from a degenerate momentum balance equation at the wall.

At

$$\eta = 0; \quad u, v, w = 0$$

$$T = T_w = 38.55°\text{C}$$

$$\partial p / \partial n = 0$$

where n is the direction normal to the body surface.

Density at the wall is computed using the field point located one radial grid point from the body after each iteration. This calculation is performed when the boundary conditions are applied.

4) Far Field Boundary: The outer boundary was selected to lie outside of the bow shock and, hence, freestream conditions were prescribed.

$$u = U_\infty \cos\alpha \qquad P_\infty = 1.724 \text{ kPa}$$

$$v = U_\infty \sin\alpha \qquad T_\infty = 95.3°\text{C}$$

$$w = 0 \qquad U_\infty = 529 \text{ m/s}$$

5) and 6) Plane of Symmetry: The two faces of the transformed unit cube lying on the plane of symmetry are represented as follows:

$$\zeta = 0 \text{ and } \pi$$

$$\frac{\partial u}{\partial \zeta} = \frac{\partial v}{\partial \zeta} = \frac{\partial p}{\partial \zeta} = \frac{\partial T}{\partial \zeta} = 0$$

$$w = 0$$

This condition was implemented numerically by matching image points which straddled the plane of symmetry.

Density of the plane of symmetry is simply computed by equivalencing the two grid points in the angular direction which straddle the plane of symmetry after one of them has been computed as a field point during a given iteration.

Initial Conditions

The computation was initiated by starting with freestream conditions ($u = U_\infty$) at $\alpha = 0$. Subsequent calculations for different angles of attack were initiated by rotating the velocity vectors of a converged solution (at $\alpha = 0$ deg) by an angle α and then applying the appropriate boundary conditions.

Transition Criteria

Before commencing with the calculations, a decision must be made as to the state of the boundary layer (i.e., laminar or turbulent) and the location of transition. The wind tunnel data compilation of Pate[13] indicates that transition on cones at zero angle of attack at a Mach number of 2 occurs at approximately a Reynolds number of 2.5×10^6. However, at angle of attack dramatic differences occur between the leeward and windward transition location. Although many parameters influence transition, Stetson[14] shows a trend with α indicating that for an angle of attack of 20 deg the following transition Reynolds numbers may be used.

	Re_{tr}	(x/d)
Leeward	0.75×10^6	1.7
Windward	3.5×10^6	8.0

Therefore for a test Reynolds number based on diameter of 0.44×10^6, the probable transition location will vary considerably (from $x/d = 1.7$ to 8.0) around the ogive cylinder. Since the major portion of the attached boundary layer (windward side) is laminar (and due to the uncertainty of the transition location), it was decided that a benchmark computation of completely laminar flow should be accomplished first as a limiting case.

Numerical Results

The case computed in this paper is a three caliber ogive with an attached cylinder and total length of ten diameters inclined at 20 deg angle of attack. The Mach number is 1.98 and the Reynolds number (based on the diameter of the cylinder) is 0.44×10^6. This set of conditions matches the wind tunnel data of Jorgensen and Perkins[2] for which a pair of symmetric vortices was observed. The wall static pressure distribution and a set of impact pressure surveys at three different stations were obtained in this experiment. A comparison of the computed results with the wind tunnel results will now be discussed.

Computed pitot pressure contours are compared with experimental values in Figs. 4, 5, and 6 at axial stations of

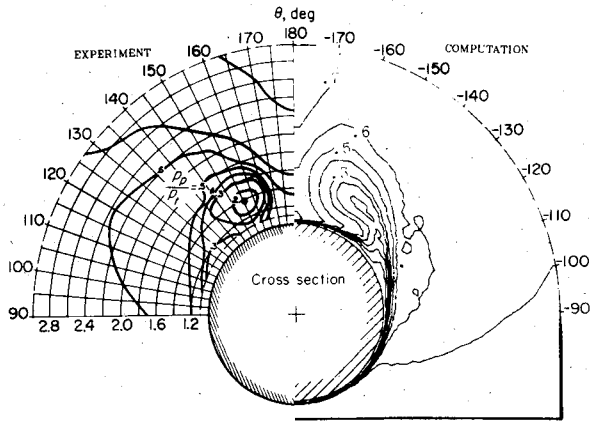

Fig. 4 Comparison of pitot pressures ($x/d = 4.5$).

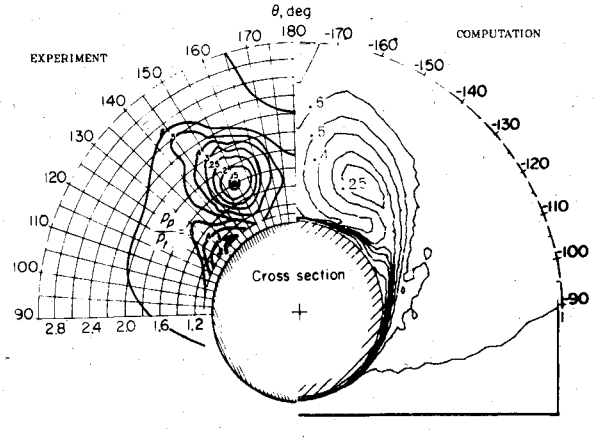

Fig. 5 Comparison of pitot pressures ($x/d = 5.8$).

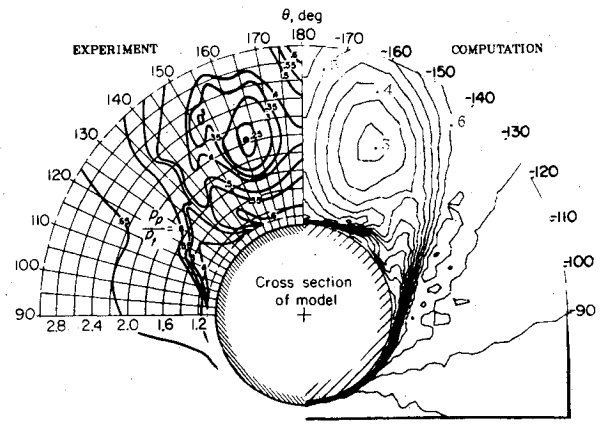

Fig. 6 Comparison of pitot pressures ($x/d = 10.0$).

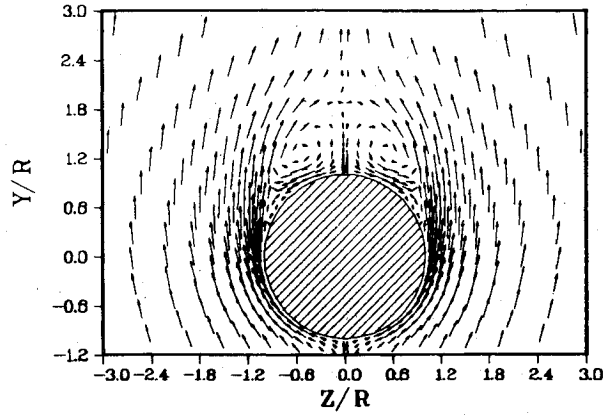

Fig. 7 Cross flow velocity vectors ($x/d = 4.5$).

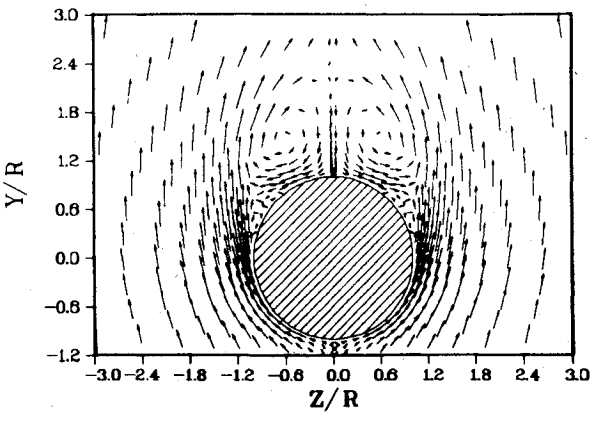

Fig. 8 Cross flow velocity vectors ($x/d = 5.8$).

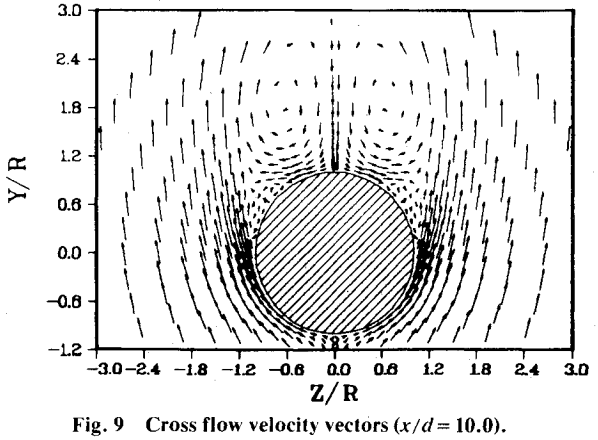

Fig. 9 Cross flow velocity vectors ($x/d = 10.0$).

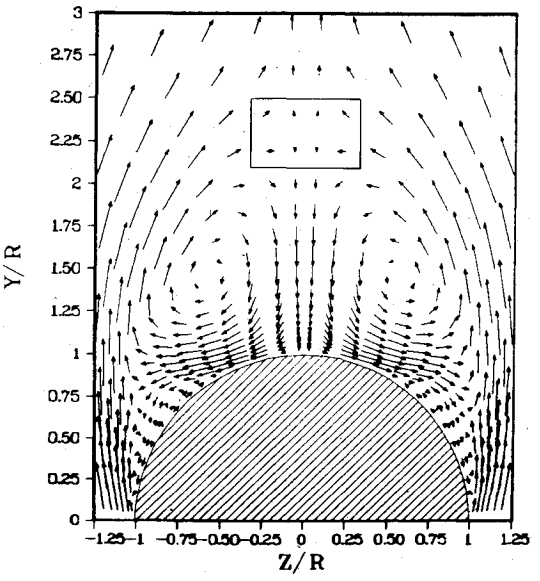

Fig. 10 Enlargement of velocity vector field ($x/d = 5.8$).

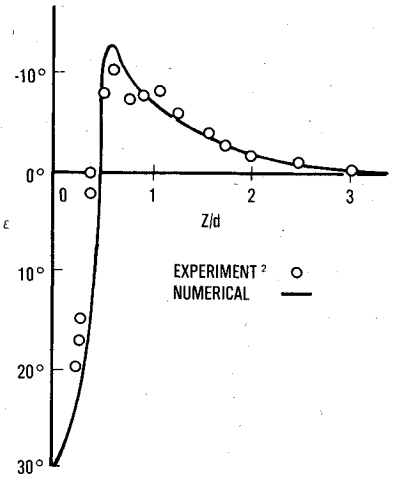

Fig. 11 Downwash angle comparison ($x/d = 5.8$, $y/d = 0.75$).

$x/d = 4.5$, 5.8, and 10, respectively. These figures display a split scene with the experiment on the left half and the numerical values on the right. The location of the vortex core is at the center of the closed contours depicting a "sink" in pitot pressure. Good agreement with the data is evident considering the qualitative nature of contouring in that interpolations must be performed from a limited amount of digital data in both the experiment and computation. The cross flow velocity vectors are plotted for the same axial stations as for the pitot pressure surveys in Figs. 7-9. Figure 10 shows an enlargement of the flowfield displayed in Fig. 8 in the vicinity of the vortex pair. The flow features about the vortex including the cross flow separation are seen clearly in these figures. An interesting aspect of this flowfield (Fig. 10) is the stagnation saddle point along the leeside plane of symmetry. Note that above the saddle point a small value of circulation exists which is opposite in sense to the primary vortex. This fact has been detected (but not explained) in experiments.[4] In Fig. 11 the downwash angle ϵ measured in a horizontal plane passing through the vortex is compared with the experiment. Outstanding agreement is observed.

A comparison of the location of the vortices (ascertained by the sink position in pitot pressure) between experiment[2,15] and the computation is shown in Fig. 12 for different axial stations. Excellent agreement with the experiment is obtained for the numerical computation.

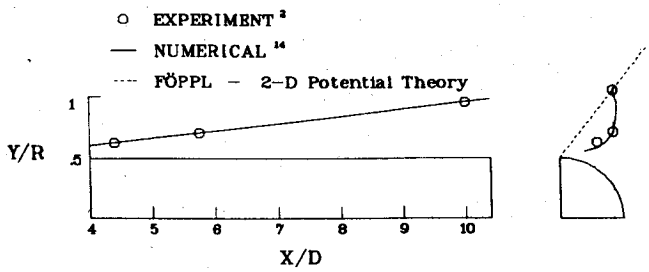

Fig. 12 Comparison of vortex center positions ($M = 1.98$).

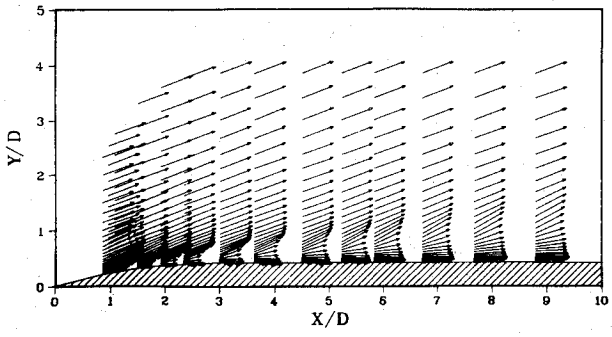

Fig. 13 Axial velocity vectors.

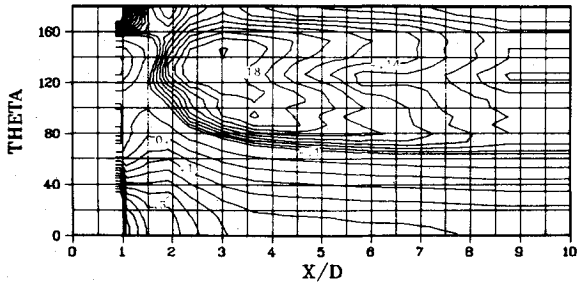

Fig. 14 Wall pressure distribution (computation).

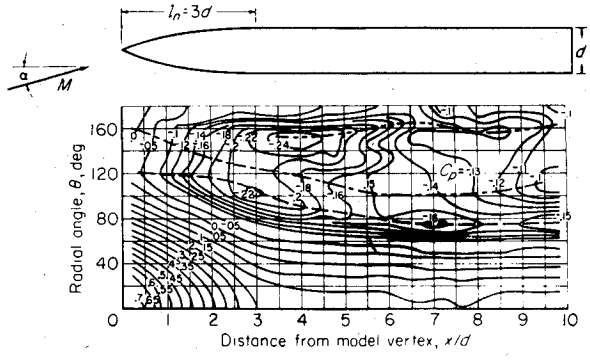

Fig. 15 Wall pressure distribution (experiment).

Although the most unusual flowfield features appear in the transverse plane, the flow is dominated by the axial velocity component. A plot of the axial velocity vectors in a ξ-η plane at a ζ-azimuthal angle (θ) of 180 deg is shown in Fig. 13. This plane cuts through the vortex core and depicts the "wakelike" character of the vortex. The computed wall static pressure contours are mapped (Fig. 14) onto the ξ-ζ plane and compared with the wind tunnel test results of Jorgensen and Perkins[2] in Fig. 15. Qualitative agreement is observed in the shape of the contours. The axial distribution of the density contours in the plane of symmetry is presented in Fig. 16. In this figure the bowshock and vortex trace can be detected. Also shown are the surface limiting streamlines in the ξ-ζ plane (Fig. 17). The convergence of streamlines near the 90-deg azimuth angle depicts three-dimensional cross flow separation. These vectors indicate the magnitude and direction of the skin friction.

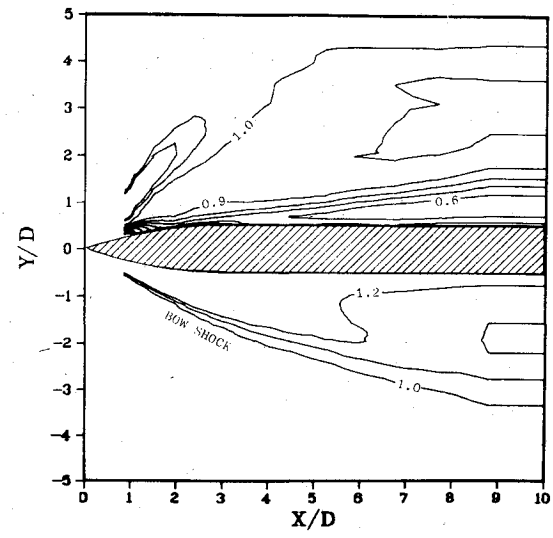

Fig. 16 Axial density contours.

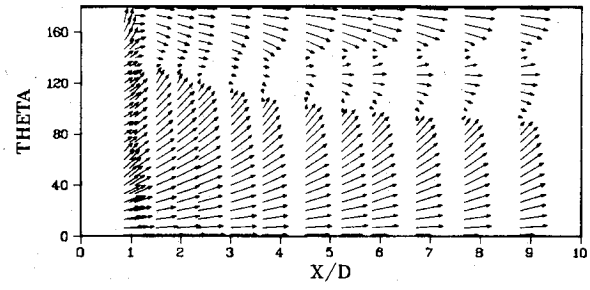

Fig. 17 Surface limiting streamlines.

Conclusions

The aerodynamic forces on slender bodies at high angle of attack depend largely upon the development of the vortex pattern on the leeside. Potential theory is not capable of uniquely determining these forces since viscous forces are essential to the process. To correctly compute the viscous phenomenon the three-dimensional Navier-Stokes equations are required. The practicality of this approach only recently became available through the advancement of the vector processor computer. Flowfield computations for laterally symmetric flow at Mach 1.98 over an ogive cylinder at 20-deg angle of attack were accomplished in 40 min on a CRAY computer, thereby demonstrating the potential for resolving problems of this nature.

The numerical computations showed good agreement with the wind tunnel data in predicting the general features of the flowfield, i.e., vortex location, separation, pressure distribution, and velocity field. Although discrepancies attributed to inadequate grid resolution or turbulent transition phenomena require further research, future emphasis shall be placed on computing the asymmetric case for which undesirable yaw forces are produced.

Acknowledgment

Air Force Weapons Laboratory, Albuquerque, New Mexico for use of their CRAY-1 computer.

References

[1] Coe, P., Chambers, J., and Letko, W., "Asymmetric Lateral-Directional Characteristics of Pointed Bodies of Revolution at High Angles of Attack," NASA TN D-7095, 1972.

[2]Jorgensen, L. H. and Perkins, E. W., "Investigations of Some Wake Vortex Characteristics of an Inclined Ogive-Cylinder Body at Mach Number 2," NACA 1371, May 1955.

[3]Tinling, B. E. and Allen, C. Q., "An Investigation of the Normal Force and Vortex-Wake Characteristics of an Ogive-Cylinder Body at Subsonic Speeds," NASA TN D-1297, April 1962.

[4]Thomson, K. D. and Morrison, D.F., "The Spacing, Position and Strength of Vortices in the Wake of Slender Cylindrical Bodies at Large Incidence," *Journal of Fluid Mechanics*, Vol. 50, Pt. 4, 1971, pp. 751-783.

[5]Calarese, W., "An Experimental Study of Vortex Flow in the Wake of a Slender Body of Revolution at Large Incidence," Air Force Wright Aeronautical Laboratories, Wright-Patterson Air Force Base, Ohio, AFWAL-TM-80-69-FIMM, May 1980.

[6]Bailey, W. H. Jr. and Calarese, W., "Experimental Study of Ogive Cylinder at $\alpha=45°$, $M=0.6$-0.7," Flight Dynamics Laboratory, Wright-Patterson Air Force Base, TM, 1981 (to be published).

[7]Chapman, G. T., Keener, E. R., and Malcolm, G. N., "Asymmetric Forces on Aircraft Forebodies at High Angles of Attack—Some Design Guides," *AGARD Conference Proceedings No. 199 on Stall/Spin Problems of Military Aircraft*, North Atlantic Treatry Organization, Nov. 1975, Ref. 12.

[8]Rakich, J. V., Vigneron, Y. C., and Agarwal, R., "Computation of Supersonic Viscous Flows Over Ogive-Cylinder at Angle of Attack," AIAA Paper 79-0131, Jan. 1979.

[9]Shang, J., Buning, P., Hankey, W., and Wirth, M., "Performance of a Vectorized Three-Dimensional Navier-Stokes Code on the CRAY-1 Computer," *AIAA Journal*, Vol. 18, Sept. 1980, pp. 1073-1079.

[10]MacCormack, R. W. and Baldwin, B. S., "A Numerical Method for Solving the Navier-Stokes Equations with Application to Shock-Boundary Layer Interactions," AIAA Paper 75-1, Jan. 1975.

[11]Shang, J. S., "Numerical Simulations of Wing Fuselage Interference," AIAA Paper 81-0048, Jan. 1981.

[12]McRae, D. S., "A Numerical Study of Supersonic Viscous Cone Flow at High Angle of Attack," AIAA Paper 76-97, Jan. 1976.

[13]Pate, S., "Effects of Wind Tunnel Disturbances on Boundary Layer Transition with Emphasis on Radiated Noise: A Review," AIAA Paper 80-0431, March 1980.

[14]Stetson, K., "Effect of Bluntness and Angle of Attack on Boundary Layer Transition on Cones and Biconic Configurations," AIAA Paper 79-0269, Jan. 1979.

[15]Owen, F. K., "Wake Vortex Measurements of Bodies at High Angle of Attack," AIAA Paper 78-23, Jan. 1978.